INTERNATIONAL ATOMIC ENERGY AGENCY
UNITED NATIONS EDUCATIONAL, SCIENTIFIC AND CULTURAL ORGANIZATION
INTERNATIONAL CENTRE FOR THEORETICAL PHYSICS
I.C.T.P., P.O. BOX 586, 34100 TRIESTE, ITALY, CABLE CENTRATOM TRIESTE

H4.SMR/449-12

WINTER COLLEGE ON
HIGH RESOLUTION SPECTROSCOPY

(8 January - 2 February 1990)

HIGH RESOLUTION SUB-DOPPLER SPECTROSCOPY

Jürgen Helmcke
Physikalisch-Technische Bundesanstalt
Braunschweig
F.R. Germnay

Winter College on High Resolution Spectroscopy
8 January – 2 February 1990, Trieste, Italy

High resolution sub-Doppler spectroscopy

Jürgen Helmcke
Physikalisch-Technische Bundesanstalt
Bundesallee 100
D-3300 Braunschweig
Federal Republic of Germany

Contents:

I. Introduction

The development of novel methods of nonlinear laser spectroscopy, high resolution frequency stabilization, cooling of ions and atoms, and optical frequency measurements have introduced strong impacts in several fields, in particular in atomic physics and frequency metrology.

Basically, the resolution of a narrow absorption feature is determined by the following line broadening effects

–the lifetime of the energy states involved in the transition (natural linewidth),
–Doppler broadening due to the velocity distribution of the thermal absorbing particles
–collision broadening reducing the undisturbed interaction time of the atoms with the light field
–power broadening causing sidebands if the Rabi frequency is large compared to the natural linewidth
–transit-time broadening caused by the limited interaction time of the absorbers with the laser beam
–the residual linewidth of the laser itself.

In these lectures we shall first discuss some basic methods of Doppler-limited spectroscopy. Till now, dye lasers are used in most applications of laboratory laser spectroscopy. Therefore we describe methods of dye laser stabilization in the third chapter and present a dye laser spectrometer which is capable of very high resolution ($\simeq$ 3 kHz). In chapter IV we discuss Doppler-free methods of laser spectroscopy for single photon transition and give a phenomenological description of saturated absorption. We shall see that surprising line shapes may be observed if we apply saturation spectroscopy to longlived transitions in an atomic beam. The highest resolution in atomic beams is observed by Ramsey's method of spatially separated excitation. With this method it is possible to resolve the recoil splitting which is in the range of a few parts in 10^{11} for most optical transitions.

This manuscript cannot give a complete description of all methods and results in Doppler-free laser spectroscopy. Very good and complete descriptions of the various aspects and methods of laser spectroscopy are given in the text books mentioned in the references [1 – 3].

II. Doppler-limited spectroscopy

In conventional absorption spectroscopy (see Fig. 1), an absorbing gas –usually contained in a cell– is illuminated by white light and the spectrum of the light which is transmitted through the cell is detected by means of a spectrum analyzer. In most cases,

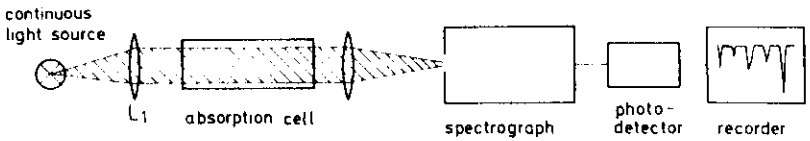

Fig. 1 Absorption spectroscopy using a white light source (taken from [1]).

the resolution is then limited by the resolving power of the spectrometer and the Doppler-limit is not reached. Furthermore, the detectable absorption is usually limited by the noise of the light source and the detector to values of $10^{-4} \geq \Delta I/I \geq 10^{-5}$.

Tunable lasers, on the other hand, with their narrow emission bandwidths provide the opportunity to probe the absorption continuously in a wide spectral range from the infrared to the ultraviolet. A typical laser spectrometer used for Doppler-limited spectroscopy is shown in Fig. 2. In this setup, the frequency of a tunable single frequency laser is scanned continuously over the absorption spectrum and the light intensity I_1 transmitted through the cell and detected by a photodetector PD 1 is recorded. The reference beam (I_2) is used to compensate intensity fluctuations of the laser source. The transmission peaks of the long Fabry-Perot interferometer are used as frequency markers for the scanning laser. Since the laser linewidth is small compared to the Doppler broadening, the resolution is Doppler limited.

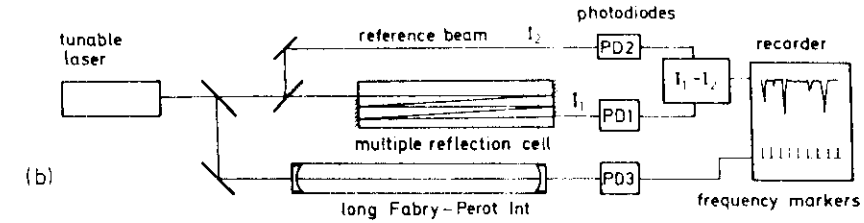

Fig. 2 Absorption spectroscopy using a tunable single mode laser (taken from [1]).

Apart from the potential higher resolution, **laser spectroscopy** provides following advantages:

- –detector noise can usually be neglected due to the high spectral power of the laser.
- –the detection sensitivity $\Delta I/I$ increases with the resolution $\omega/\Delta\omega$ as long as the detection bandwidth is larger than the absorption line.
- –the good collimation of the laser beam allows multiple passes through the absorption cell which is important for small absorption coefficients.
- –absorption spectroscopy can be used to stabilize the frequency of lasers providing references for spectroscopy and metrology.
- –profiles of absorption lines can be measured with high accuracy.
- –the high intensity of the lasers can be used to change the population of the absorbing gas to excited states allowing nonlinear methods of laser spectroscopy (saturated absorption, two photon spectroscopy, optical pumping,...).

The absorption coefficient per length x $\alpha(\omega)$ is defined by the relation

$$I_T(\omega) = I_0 \cdot \exp[-\alpha(\omega)x].$$

For small absorptions $\alpha(\omega)x \ll 1$ is

$$I_T(\omega) \simeq I_0[1-\alpha(\omega)x]$$

and we can write

$$\alpha(\omega)x = |I_0 - I_T|/I_0.$$

Small absorption coefficients can therefore be recorded by measuring the small difference of large intensities. In these cases the uncertainty depends critically on the splitting ratio of the reference beam (see Fig. 2). Furthermore, spurious interferences –caused for example by scattered laser light– may also influence the detected signals. Several methods have been developed to reduce such detrimental effects.

The first method employs frequency modulation of the laser and phase-sensitive detection of the transmitted intensity (see Fig. 3). The value $I_T(\omega+\Delta\omega) - I_T(\omega)$ can be expanded into

$$I_T(\omega+\Delta\omega)-I_T(\omega) = (dI_T/d\omega)\Delta\omega + \frac{1}{2!}\frac{d^2 I_T}{d\omega^2}\Delta\omega^2+\ldots \cong -I_0 x \frac{d\alpha(\omega)}{d\omega}\Delta\omega+\ldots$$

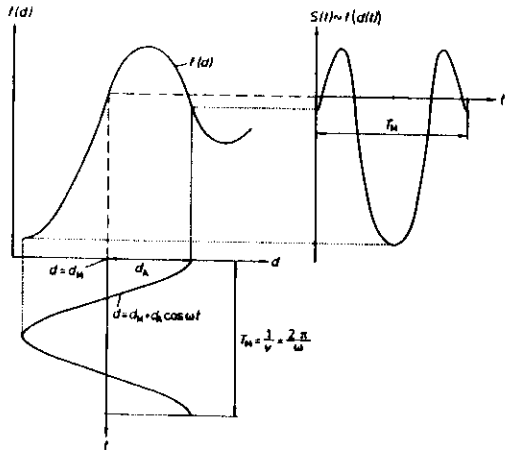

Fig. 3 Principal setup of the method of frequency modulation

If the modulation width $\Delta\omega$ is small compared to the width of the spectral structure, the first term of the expansion is proportional to the first derivative of the absorption

$$\frac{d\alpha(\omega)}{d\omega} = \frac{-1}{I_0 x}\frac{dI_T}{d\omega}.$$

High sensitivity can then be achieved by means of phase sensitive detection allowing small detection bandwidth (long time constants for signal integration). To improve the

signal-to-noise ratio, the modulation width $\Delta\omega$ is often of the same order of magnitude as the spectral feature to be observed. In these cases the first harmonic used for the detection can be derived from a Fourier expansion [4].

A second method –very sensitive in the visible and ultraviolet range– monitors the absorbed power directly by detecting the laser excited fluorescence. This method is shown schematically in Fig. 4. It is frequently applied in collimated atomic/molecular beams where the absorbed power is extremely small due to the low density of absorbers and the small absorption length x. In this scheme, the excited atoms decay by emission

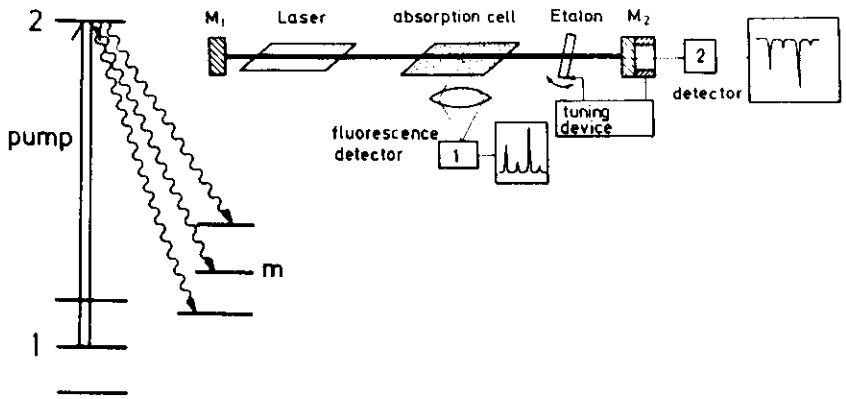

Fig. 4 Principal setup for fluorescence detection (taken from [1]).

of radiation into a lower state and the intensity of the radiation is measured. If the laser frequency ω_L is tuned to an absorbing transition, the number of photons n_a absorbed per second and path-length Δx is

$$n_a = N_i \sigma_{ik} n_L \Delta x$$

where N_i is the density of absorbers in the initial state, σ_{ik} the absorption cross section per absorber, and n_L the number of incident photons. If all laser excited absorbers decay under emission of one photon, the number of fluorescence photons n_{fl} emitted per second is given by

$$n_{fl} = N_k A_k = n_a$$

where N_k is the excited state density and A_k the total probability for spontaneous emission. The fluorescence intensity detected by the photomultiplier is reduced due to the quantum efficiency of the photocathode η_{Ph} and due to the limited collection

efficiency δ. Assuming $\eta = 0.2$ and $\delta = 0.1$, single photon counting, and a dark counting rate of the photomultiplier of 10 s^{-1}, the minimum detectable rate of fluorescence photons (S/N = 1) is given by $n_{fl\ min} = 500\ s^{-1}$. For a wavelength of 500 nm this value corresponds to a minimum detectable power of $P_{fl\ min} = h\,\nu\,n_{fl\ min} \simeq 2 \cdot 10^{-16}$ W.

III. High resolution dye laser spectrometer

High resolution laser spectroscopy requires stable (narrow bandwidth) lasers of which the frequency can be tuned precisely. In most applications dye lasers or color center lasers are employed. They can operate continuously at a single frequency making available any transition in the visible range. Single frequency output powers of more than one Watt have been reported. The spectral range of these lasers can be further extended by frequency mixing or frequency doubling. In the following we shall concentrate ourselves on dye lasers (the "working horses" in laser spectroscopy).

A typical setup of a single frequency dye ring laser is shown schematically in Fig. 5. In principal, the dye laser consists of an amplifying dye jet stream which is pumped by a high power ion laser. This jet is positioned inside an optical resonator which in Fig. 5 consists of five mirrors and a Mach-Zehnder interferometer (MZI). The laser frequency is roughly determined by means of a birefringent filter and a thin etalon (FSR ≃ 670 GHz).

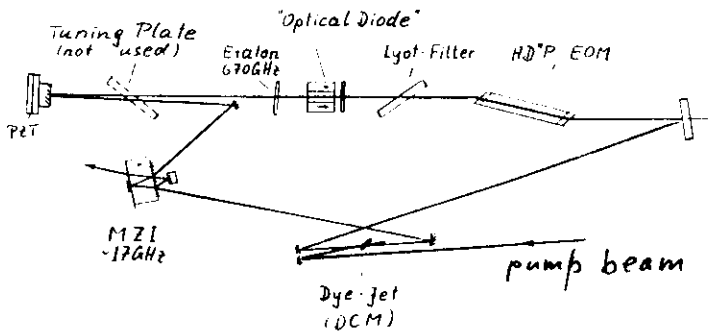

Fig. 5 Scheme of the PTB dye laser designed for high resolution laser spectroscopy

The MZI selects the correct cavity order. Travelling wave operation in one direction of the ring resonator is achieved by means of an optical diode (unidirectional device). The frequency of the dye laser can be changed by applying voltages to an ADP electro-optical phase modulator (fast changes) and to the PZT of one of the mirror mounts.The fast dye stream inside the laser cavity causes fast thickness fluctuations of the jet which are showing up as frequency fluctuations of the emitted radiation and resulting in an increased laser linewidth of a few MHz. Line narrowing can be achieved by stabilizing the laser frequency to a resonance of a stable optical (reference) resonator. With this method, the linewidth can be reduced by several orders of magnitude. Frequency scanning can then be performed either by scanning the frequency of the optical resonator or by applying optical modulation techniques.

Fast frequency stabilization to an optical resonator.

The design of a suitable frequency stabilization requires the knowledge of the frequency noise spectrum of the laser. A typical spectrum is shown in Fig. 6. This spectrum extends up to frequencies of several hundred kHz. Correspondingly, a fast servo system is

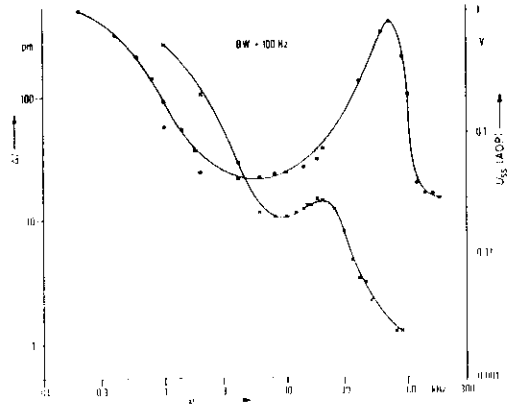

Fig. 6 Typical spectral density of the frequency fluctuations of a free running dye laser.

needed to reduce the frequency noise efficiently. A simple stabilization method is shown in Fig. 7a. In this setup, the laser beam used for the stabilization is split into a reference beam I_r and a signal beam I_s mode matched into the cavity. The power of the reference beam is aligned to about one half of the power transmitted through the cavity at the

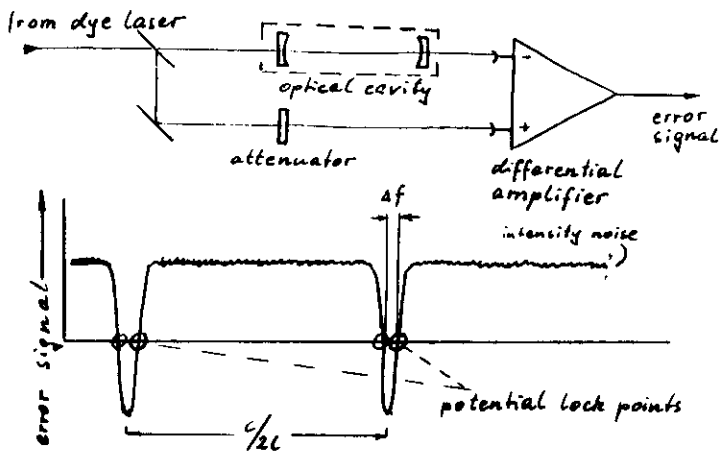

Fig. 7 a) Typical setup for the frequency stabilization of a dye laser to the half point of a cavity fringe. b) Typical error signal versus the laser frequency. The marked points can be used as references for the stabilization.

center of its resonance. The difference of the detected signal is shown in Fig. 7b. There are two zero crossings at the half points of the cavity resonance. Either of these points can be used as error signals for the frequency stabilization. After suitable integration, this signal is used to correct the optical length of the cavity. With this method, laser linewidths below ten kHz have already been observed using fast servo electronics [5,6].

Method of phase modulation

The narrowest laser linewidths are observed by means of a "phase–modulation (pm) method" [7] shown in Fig. 8. This stabilization method was first applied to microwave oscillators. For the stabilization, part of the laser beam is split off the main laser beam and mode–matched into an optical resonator. The incident beam is phase modulated by means of an electro-optic modulator (EOM). The modulation frequency in the range of 10 MHz to 20 MHz should be larger than width of the cavity resonance. After reflection at the resonator, the phase modulation is partially converted to a power modulation which contains information about the offset from the center of the cavity resonance. This power modulation is phase–sensitively detected by means of a photodetector (PD), amplified and sent to a double–balanced mixer (DBM) which is driven at the modulating frequency. The detected photo signals are depicted in Fig. 9.

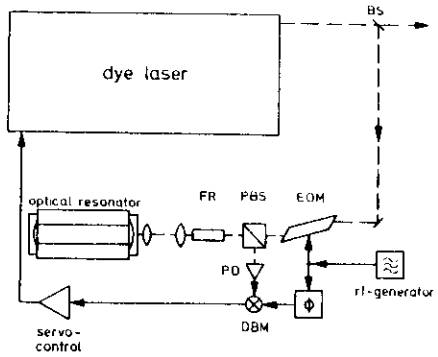

Fig. 8 Frequency stabilization of a dye laser to an eigenfrequency of an optical resonator by the method of phase modulation.

The curves "a" and "b" show the transmitted and the reflected powers, respectively, as functions of the laser frequency. The carrier and the adjacent sidebands of the phase modulation are clearly resolved. Figs. 9c and 9d represent the demodulated signals at the output of the mixer: "c" is in phase and "d" is in quadrature with the modulation at the EOM. The zero–crossing of the central part of the dispersion like curve (c) coincides with an eigenfrequency of the resonator. This dispersion signal is used as error signal for the stabilization. Laser linewidths below 1 Hz with respect to the eigenfrequency of the resonator have recently been reported [8 – 10]. In the cases of refs. 9 and 10, these linewidths were estimated from the error signal indicating that the electronic servo system is capable of sub-Hz resolution, in principle. The frequency at unity servo gain was in the range between 2 MHz and 3 MHz. Compared to the stabilization method described before, the phase-modulation method offers the following advantages:

–the frequency is locked to the center of the resonance rather than to the wing,

–the detection band is transformed into a frequency range where technical laser noise can be neglected.

–the capture range of the servo-control is increased to the value of the modulation frequency which is larger than the cavity resonance width.

–the servo-bandwidth can be larger than the resonance width since the transient

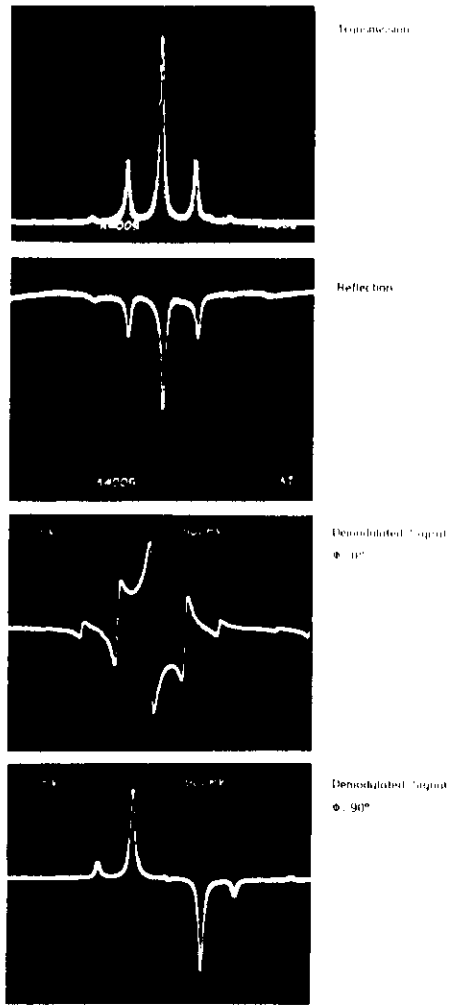

Fig. 9 Photosignal vs laser frequency observed by means of the phase modulation method. Photocurrent transmitted through the cavity (a), reflected at the cavity (b). Demodulated signals at the output of the DBM in phase (c) and in quadrature (d) with the voltage at the EOM.

behavior of the cavity is described by an integrating behavior which can easily compensated by the servo-control.

Longterm stabilization and precise frequency tuning

The frequency of the "cavity stabilized" dye laser depends on the stability of the reference cavity itself. At PTB, we have developed a "solid-ingot" resonator consisting of the low expansion material "zerodur" (see Fig. 10). The zerodur mirrors are optically contacted to the zerodur spacer. The cavity is hanging on five thin wires in a temperature stabilized vacuum container [7]. This support system is used to avoid that noise of the optical table couples into length variations of the cavity. Presently, the resonance width of our reference cavity is approximately 700 kHz (FWHM). The longterm stability of the cavity has been measured by stabilizing a single frequency He-Ne to a suitable cavity resonance and measuring the beat frequency against an iodine

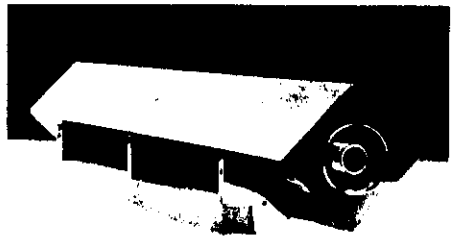

Fig. 10 Reference resonator.

stabilized He-Ne–laser used as frequency reference (see below). The corresponding frequency change is shown versus time for an interval of almost two years in Fig. 11. Presently the drift rates are in the range of approximately 2 Hz/s. However during data acquisition when local heating of the resonator may occur, this drift rate can be more than ten times higher.

Fig. 12 shows a block diagram of a dye laser spectrometer developed at PTB for the

investigation of super-narrow spectral structures. With our spectrometer care was taken to address the problems of longterm stability, repeatability, and precise frequency

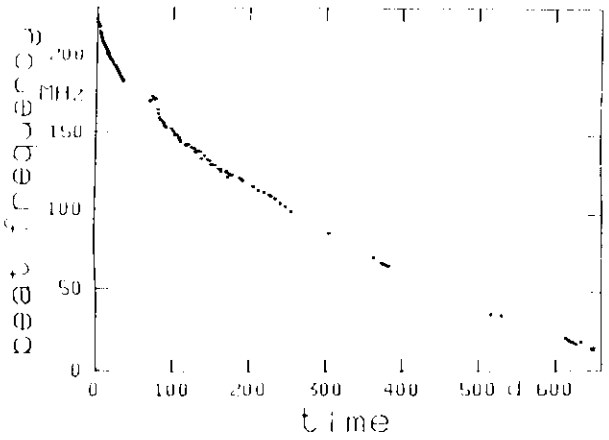

Fig. 11 Change of the resonance frequency of a Zerodur optical cavity vs time (λ = 657 nm)

scanning. For stabilization, part of the laser beam is first focused into an acousto–optic modulator (AOM). The Bragg–reflected beam is then retroreflected coaxial, phase modulated and mode matched into the cavity. In this way the light beam incident into the resonator is shifted by twice the frequency ν_m driving the AOM. Using a servo bandwidth of 2.5 MHz at unity gain for frequency stabilization, the rms laser linewidth was in the range of 1 kHz. This linewidth was deduced from the spectrum of the beat frequency between the dye laser and a He-Ne laser, both frequency stabilized to their individual reference cavities. Precise frequency scanning of the laser is performed by tuning the modulating frequency ν_m. Residual drifts of the resonator are detected by measuring the beat frequency ν_b between a He-Ne laser stabilized to a resonance of the cavity and an I_2–stabilized He-Ne laser. The resonator drift is compensated automatically by correcting ν_m according to the equation $\delta\nu_m = \delta\nu_b(\lambda_{HeNe}/\lambda_{dye})/2$ ($\delta\nu_m$: frequency correction applied to the AOM, $\delta\nu_b$: change of the beat frequency between the two He-Ne lasers, λ_{HeNe} and λ_{dye}: wavelengths of the He-Ne laser and the

dye laser, respectively).

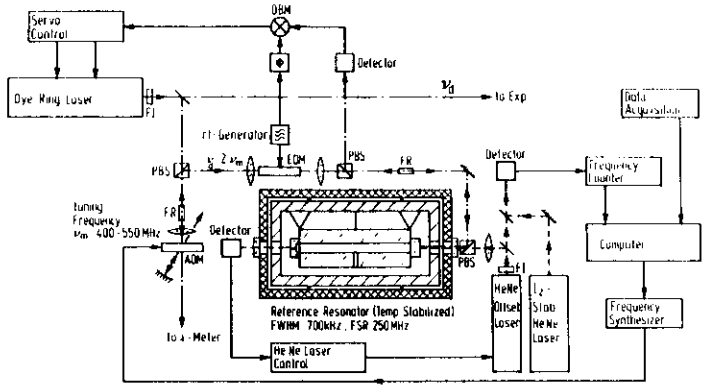

Fig. 12 Ultra-high resolution dye laser spectrometer [11].

With this spectrometer the frequency fluctuations of the dye laser within a time interval of approximately six hours were less than ± 2.5 kHz. During several months, the frequency of the spectrometer could always be reset to the same value within ± 10 kHz. Presently, the useful spectral resolution of approximately 3 kHz is limited by the residual frequency instability of the I_2–stabilized He-Ne laser.

IV. High resolution sub-Doppler spectroscopy.

Doppler broadening

Usually, the Doppler broadening provides by far the largest contribution to the line

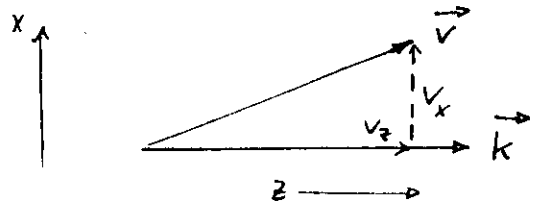

Fig. 13 Doppler effect of an atom moving at a velocity v.

broadening. In the frame of an atom moving at a velocity v and under an angle α to a laser beam of the frequency ν_L (see Fig. 13) the frequency can be expressed as

$$\nu_a = \nu_L[1 - (v/c)\cos\alpha + v^2/(2c^2)].$$

In this equation, the term $(v/c)\cos\alpha$ represents the linear Doppler effect. It is proportional to the velocity component v_z in the direction of the laser beam. Note that the sign of the linear Doppler shift reverses if the direction of the laser beam or the velocity is reversed. The third term which is quadratic in v and independent of the velocity direction represents the second order (relativistic) Doppler effect.

The atomic velocities along a fixed direction of a gas in thermal equilibrium at a temperature T can be expressed by the Maxwellian distribution

$$w(v) = 1/(\sqrt{\pi}\, u)\exp[(-v^2/u^2)]$$

with

$$u^2 = 2KT/m$$

where K represents the Boltzmann constant and m the atomic mass. This Gaussian velocity distribution causes a Doppler-broadened linewidth of a Gaussian profile if other line broadenings can be neglected. In this case, the absorption profile is expressed as

$$\alpha(\omega) = \alpha_0 \cdot \exp[-(\omega - \omega_0)^2/(\omega_0 u/c)^2]$$

and the Doppler width (HWHM) is

$$\Delta\omega_D = \frac{\omega_0\, u}{c}\sqrt{\ln 2} = 0.833\ \omega_0\, u/c.$$

The Doppler width of most gases at room temperature is usually in the range of $10^{-6}\omega$. Whereas the second order Doppler effect is in the range of $10^{-12}\omega$. We shall see later that at very high resolution, the uncertainty to find the true line center is limited mostly by the second order Doppler effect.

Collimated atomic beams

We have seen that the first order Doppler shift depends on the direction of the atomic

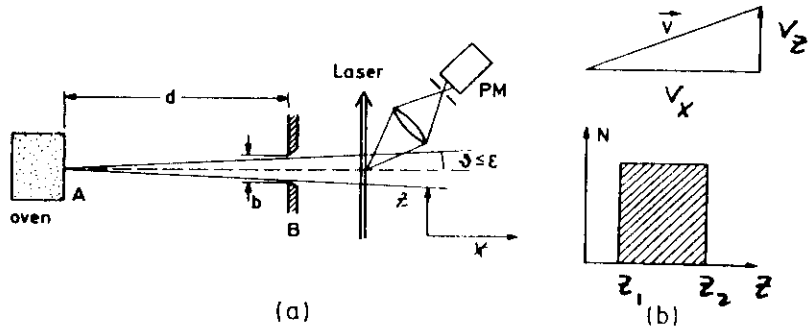

Fig. 14 Illustration of Doppler-reduced laser spectroscopy using an atomic beam (taken from [1]).

velocity relative to the laser beam. It vanishes if the atoms cross the light beam under a right angle. In a gas cell, the atomic velocities are isotropically distributed in all directions and no Doppler suppression is expected in linear spectroscopy. On the other hand, collimated atomic beams [12] crossing perpendicularly with a monochromatic laser beam provide the opportunity to reduce the Doppler-broadening to a high degree. Collimation ratios of 1/1000 are easily achieved. Fig. 14 shows a schematic setup of such an experiment. The collimation of the atoms leaving the atomic beam source (oven) is provided by an aperture B at a distance d from the source. For a point source, the collimation ratio is $b/d \simeq v_z/v$. The Doppler-shifted frequency (first order Doppler-effect) in the rest-frame of the moving atom is

$$\omega_0' = \omega_0 - \vec{k}\cdot\vec{v} = \omega_0 - kv_z$$

where $\vec{k}$ ($|k| = 2\pi/\lambda$) is the wave vector. Only those atoms with a velocity component

$$v_z \leq \frac{1}{2}|v|\, b/d$$

can contribute to the absorption of the monochromatic laser beam and the corresponding Doppler-shift is reduced approximately by the collimation ratio to $\delta\omega_D = k\, v_z$.

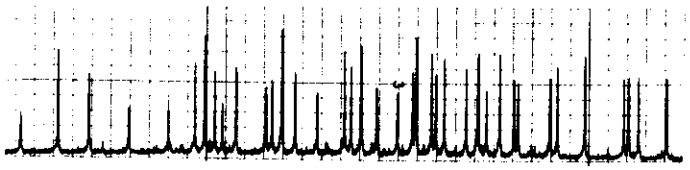

Fig. 15 High resolution spectrum of molecular iodine observed in a molecular beam by means of laser fluorescence spectroscopy [12].

Fig. 15 shows a typical absorption spectrum of iodine observed at $\lambda = 514.5$ nm observed by exciting a molecular iodine beam with a single frequency argon-ion laser [12]. The absorption peaks represent narrow hyperfine structure components (HFS) of the P(13) (43 − 0) and the R(15) (43 − 0) lines of the electronic B − X transition. Since the separation of the HFS components is smaller than the Doppler width they could only be resolved by means of sub-Doppler spectroscopy.

Saturation Spectroscopy

Saturation spectroscopy is based on the selective saturation of a certain velocity group of an inhomogeneously broadened line. As it is shown in Fig. 16, the velocity component v_z of an absorbing gas is selected by the laser frequency ω_L according to the condition

$$v_z \pm dv_z = (\omega_0 - \omega_L \pm \delta\omega)/k$$

Because of the depletion of the population difference $\Delta n(v_z)$ the absorption coefficient $\alpha(\omega) = \Delta N(v_z)\sigma_{ik}\ (\omega_0 - \omega - v_z k)$ decreases from its unsaturated value $\alpha_0(\omega)$ to the saturated value

$$\alpha_s(\omega) = \alpha_0(\omega)/\sqrt{1+S_0}.$$

Where $S_0 = P/P_s$ is the saturation parameter (P_s: saturation power) at line center. Since the the absorption coefficient α_s depends on the laser intensity, the absorbed power depends nonlinearly on the laser power. Therefore saturated absorption is called a

nonlinear method of laser spectroscopy.

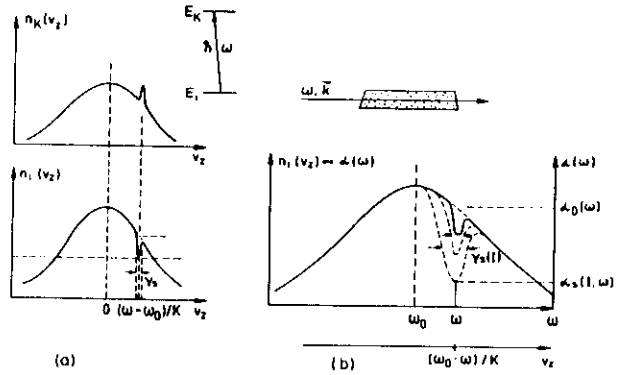

Fig. 16 Hole burning in the initial level and corresponding population peak in the excited level of a Doppler-broadened line (taken from [1]).

Doppler-free saturation spectroscopy makes use of the fact that the absorption coefficient of a gas can be saturated at a certain velocity, selected by the laser frequency ω_L. This narrow hole can be probed selectively, for example, with a second laser beam of which

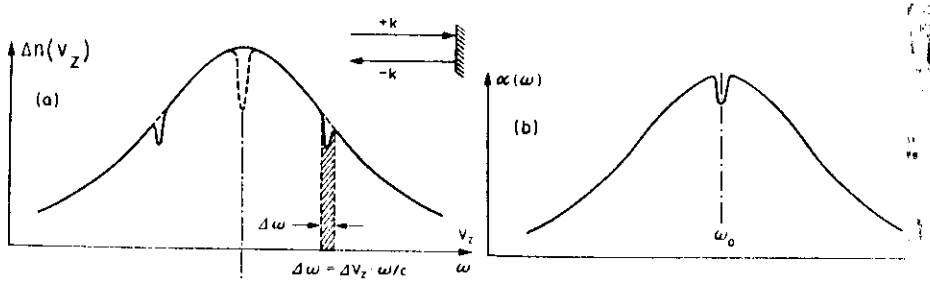

Fig. 17 Saturation holes "burned" symmetrically into the velocity distribution by two counterpropagating waves (taken from [1]).

the frequency is scanned over the Doppler-broadened line profile. At low intensities, the width of this "Bennett hole" [13] equals the natural linewidth of the transition (if further broadenings can be neglected). If the laser beam is retroreflected after leaving the cell, the retroreflected beam generates a second hole into the population distribution placed symmetrically to the line center at $v_z = 0$ (see Fig. 17). If the laser frequency is tuned, these holes move symmetrically to $v_z = 0$. At line center, both holes overlap and the number of atoms available for absorption is reduced. Consequently, one observes a narrow Doppler-free absorption dip when the laser frequency is tuned over the center of the Doppler-broadened line. Fig. 18 shows a typical experimental arrangement for saturation spectroscopy. The laser beam is split into a pump and a probe beam. Both beams are passing through the cell in (almost) opposite directions. The power of the probe beam is detected versus the laser frequency after passing the cell. Chopping of the pump beam allows to detect the difference of the power absorbed in the probe beam when the pump beam is turned on and off (i.e. the nonlinear part of the absorption, containing the Doppler-free signal). This can be performed by phase sensitive detection.

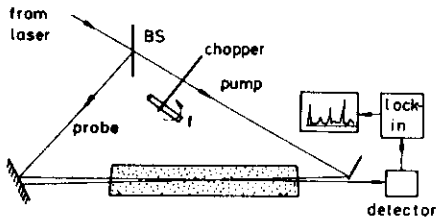

Fig. 18 Experimental arrangement for saturation spectroscopy.

Saturated absorption has been applied successfully using laser intra-cavity absorption cells. A typical example is the iodine stabilized He-Ne laser operating at 633 nm wavelength (see Fig. 19). This laser is frequently used as a precise wavelength standard in spectroscopy (see dye laser spectrometer above) and length metrology. The emission line of the laser coincides with the R(127) line of the 11 – 5 band of $^{127}I_2$. The condition of counterpropagating waves is automatically fulfilled in a linear standing wave laser resonator. The laser resonator contains the He-Ne gain tube and the iodine absorption cell. The frequency of the laser can be changed within the Doppler-width of the gain

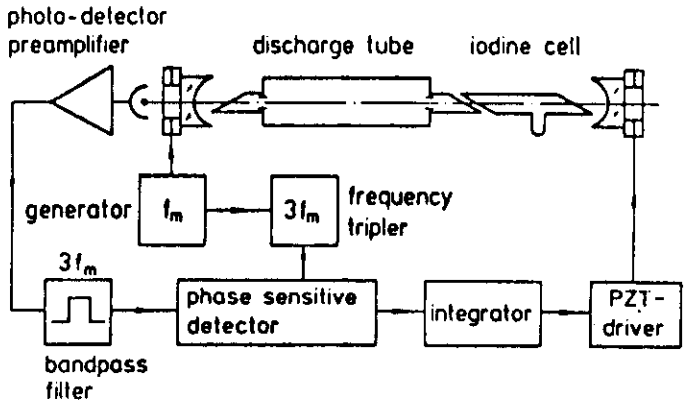

Fig. 19 Schematic setup of an I_2-stabilized He-Ne laser (λ = 633 nm).

profile by moving one of the mirrors mounted on PZT-transducers. The output power increases when the laser frequency is tuned to the center of a corresponding absorption line (see Fig. 20a). Intracavity saturated absorption provides very high sensitivity due to

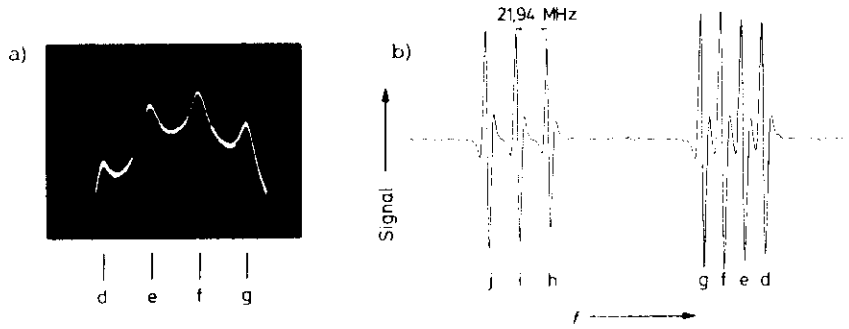

Fig. 20 a) Output power of an iodine stabilized He-Ne laser vs the cavity length. The size and width of the dips are approximately 0.1% of the output power and 10^{-8} of the laser frequency. b) Absorption spectrum observed by using the third harmonic detection technique.

the strong dependence of the laser output power on cavity losses near the laser threshold. To find the true line center, the effects of a sloped background needs to be suppressed. This can be done by applying the "third harmonic detection technique" [14,15]. For this purpose the laser frequency is modulated by applying a harmonic voltage to the PZT of the second mirror-mount. In the vicinity of the absorption line, the output power will then be also modulated with the modulation frequency and its harmonics. For a symmetrical line all odd harmonics will show a zero crossing and a phase change of π when the frequency is tuned through the center of the resonance. If we assume that the background can be approximated by a linear and a quadratic term, the signal containing the third harmonic will not be influenced by the background and can be used to generate an error signal for the frequency stabilization. Therefore, the third harmonic is selected from the photo-current, amplified, and phase-sensitively detected. The servo-loop is then used to control the length of the cavity such that the third harmonic signal vanishes. Using this setup, frequency reproducibilities in the range of a few $10^{-11}\nu$ have been achieved at several international laser comparisons between various lasers of different metrological institutes [16,17,18].

Phase-modulation spectroscopy

Even though intracavity saturation spectroscopy provides a very sensitive tool to detect very small absorption features with high accuracy, this method cannot be applied in every case. For example, intracavity absorption cells would prevent low-gain lasers to oscillate. Furthermore, in intra-laser-cavity saturated absorption the signal profile depends on a variety of operation parameters which can hardly be separated experimentally.

A very sensitive method closely related to saturation spectroscopy is provided by phase-modulating the probe beam. Using modulation frequencies above the range where technical laser noise can occur (usually above a few MHz), shot-noise limited detection can be achieved. The method of phase-modulation was first introduced by Bjorklund [19] and Hall et al. [20]. A typical setup for Doppler-free phase-modulation spectroscopy is shown in Fig. 21 [20]. This setup is very similar to the one shown in Fig. 18. However, the chopper of the pump beam is replaced by an acousto-optic modulator (AOM) which frequency offsets the pump frequency and allows higher chopper frequencies. Furthermore, the probe beam is phase-modulated at a frequency high

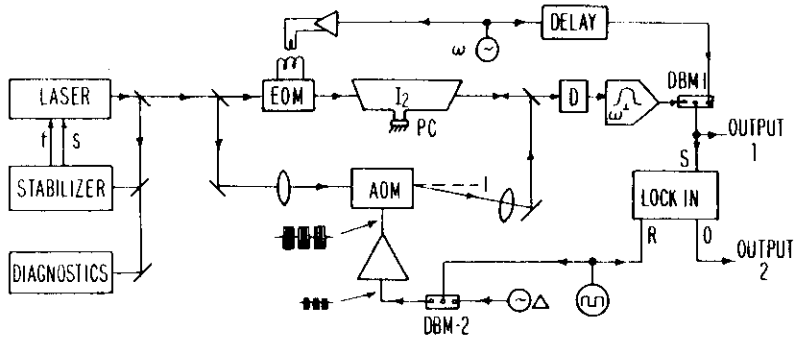

Fig. 21 Experimental setup used for Doppler-free phase-modulation spectroscopy (taken from [20]).

compared to the linewidth. The superposition of the two counterpropagating waves

$$E_1 = E_0 \cdot \exp\,[i\omega\,(t - z/c]$$

and $$E_2 = E_0 \cdot \exp\,[i(\omega + \Delta\omega)(t + z/c)]$$

results in a "walking wave"

$$E_1 + E_2 = 2\,E_0 \cdot \exp[i\omega t\,(t + z/c)\Delta\omega/2] \cdot \cos[\Delta\omega t/2 + (\omega + \Delta\omega/2)z/c]$$

of which the nodes and antinodes move at a velocity of

$$v_w = \Delta\omega\, c/(2\omega + \Delta\omega) \simeq \Delta\omega\, c/(2\omega)$$

Atoms moving with a velocity component $v_z = v_w$ "see" both counterpropagating beams at the same frequency. In this frame we have again the case of saturated absorption. Correspondingly, the laser frequency at resonance is Doppler-shifted by $\omega \cdot v_w/c$ which is half of the frequency applied to the AOM. With the pump beam being frequency offset, any interference between the probe beam and light of the pump beam being scattered into the detector occurs at the offset frequency and does not fall into the detection bandwidth [21]. Chopping of the pump beam is provided by modulating the rf-power applied to the AOM. The chopping frequency has to be smaller than the linewidth in order to allow the atomic population to follow.

Sensitive probing of the saturation dip is provided by phase-modulating the probe beam before it enters the absorption cell. When the probe beam crosses the hole burned into the velocity distribution of the population difference, the phase modulation is partially

transformed into a power modulation which can be detected phase-sensitively (see the chapter of dye laser stabilization).

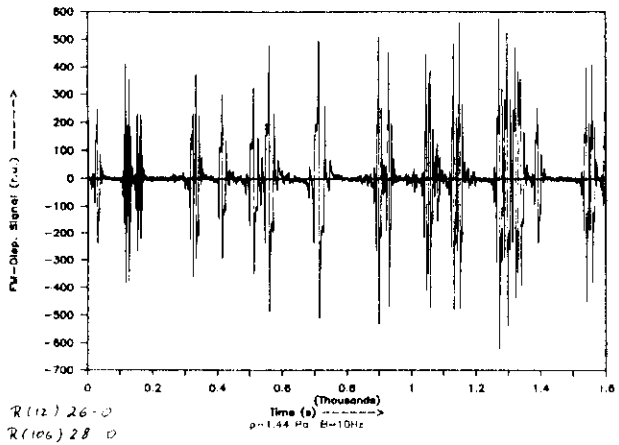

Fig. 22 HFS spectrum of iodine observed by phase-modulating spectroscopy in the emission range of a He-Ne laser of 543.5 nm wavelength [22].

At PTB, we have used this technique to stabilize the frequency of an He-Ne laser, operating at λ = 543.5 nm, to iodine absorption features [23]. In this case intracavity saturation spectroscopy was impossible due to the very low gain of the laser transition and due to the fact that only lasers with integrated mirrors were available at that time. Fig. 21 shows the iodine absorption spectrum observed with this technique. It should be noted that only 90 μW and 37 μW were available for the pump and the probe beam, respectively, to record these spectra. Two lasers stabilized independently by this method gave the same frequency within approximately 1 kHz.

Crossover transitions in saturation spectroscopy

In the saturation experiments discussed above, only two levels have been involved. In many applications however such a two-level atoms may not provide a realistic description. In a three level atom for example (see Fig. 23), where one level (a) can couple with the two others (b and c) then a further resonance, the "crossover transition"

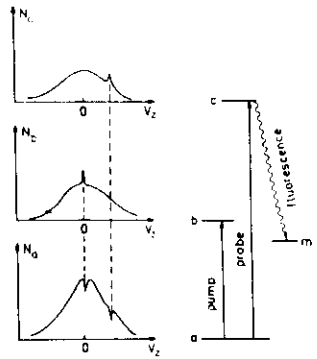

Fig. 23 Energy diagram of a three-level atom enabling crossover resonances (taken from [1]).

can occur. In the frame of a three level atom moving with the velocity component v_z (see Fig. 23 a) the two counterpropagating waves have the frequencies

$$\omega_- = \omega_L(1 - v_z/c + ...)$$

for the wave copropagating with v_z and

$$\omega_+ = \omega_L(1 + v_z/c + ...)$$

for the counterpropagating one. Doppler-free crossover signals can be observed if

$$\omega_- = \omega_{ab} \text{ and } \omega_+ = \omega_{ac}.$$

This condition is fulfilled if

$$\omega_L = (\omega_{ac} + \omega_{ab})/2$$

and

$$v_z/c = (\omega_{ac} - \omega_{ab})/(\omega_{ac} + \omega_{ab})$$

The crossover resonance is observed if the laser frequency is tuned to the mean of the two transition frequencies $\omega_L = (\omega_{ab} + \omega_{ac})/2$. It is clear that such crossovers can only occur if the difference $\omega_{ac} - \omega_{ab}$ is smaller than the Doppler width.

Saturated absorption spectroscopy in an atomic beam

The width of spectral profiles observed by saturated absorption in absorption cells is frequently determined (for small natural line widths) by collisions between the atoms. Such collisions can be reduced to negligible values by using atomic/molecular beams. Even though linear spectroscopy using atomic beams is capable of sub-Doppler resolution, the line may still be inhomogeneously broadened due to the residual velocity distribution in the direction of the propagating wave v_z. The application of saturated absorption in atomic beams allows to suppress the influence of collisions efficiently. Due

to the smaller Doppler width, crossover transitions can also be avoided in many cases. If the lifetime of the levels involved in the transition is long enough, probe and pump beams can be spatially separated. Such experiments were performed at the Ca intercombination line $^3P_1$-$^1S_0$ (λ = 657 nm) of which the excited $^3P_1$-level has a long life time of approximately 0.5 ms (see chapter V). The experimental setup is shown in Fig. 24.

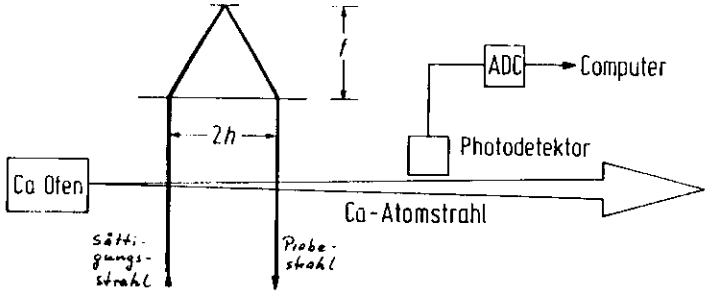

Fig. 24 Experimental setup for saturation spectroscopy in a Ca atomic beam

We shall see in later that at high laser powers the corresponding line profile depends strongly on the excitation geometry i.e. whether a standing wave or two counterpropagating travelling waves are applied [24].

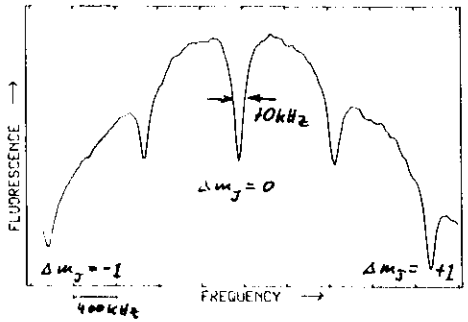

Fig. 25 Saturated absorption signal observed in a Ca atomic beam.

Fig. 24 shows a typical setup for saturated absorption spectroscopy in a calcium atomic beam. The collimated laser beam (w = 1.5 mm) from a dye laser spectrometer crosses the Ca beam perpendicularly and it is retroreflected by a cat's eye. The cat's eye can be

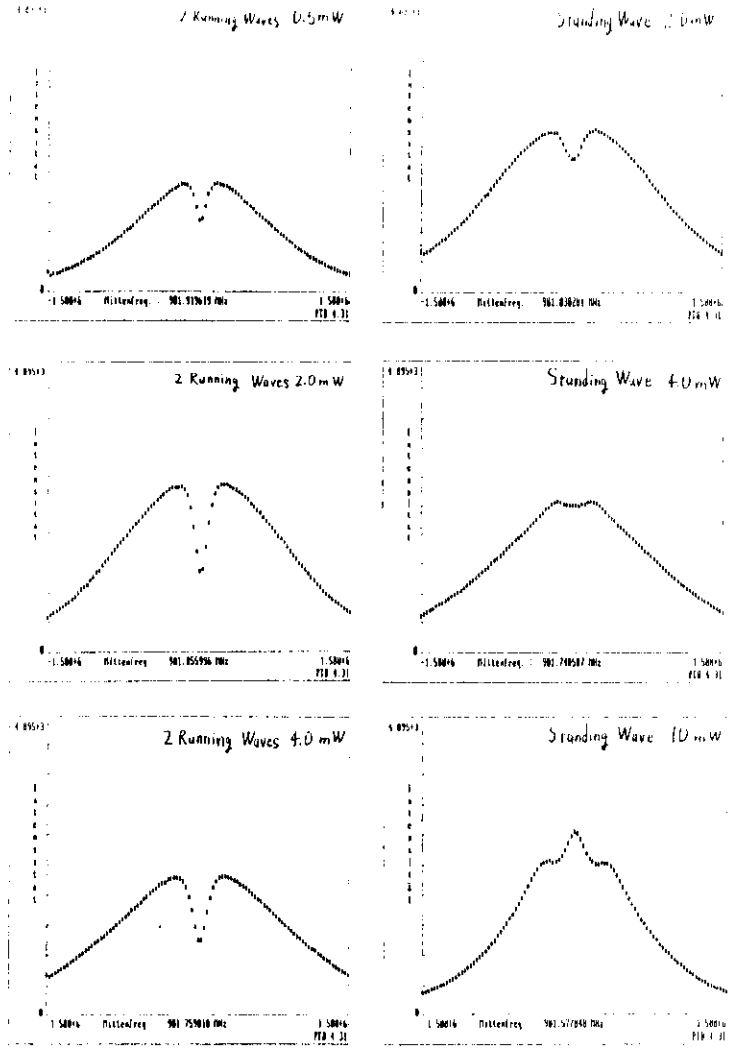

Fig. 26 Saturated absorption features observed in a Ca atomic beam for excitation by a standing wave (a) and two counterpropagating travelling waves (b) [24]

moved parallel to the Ca atomic beam thereby changing the distance between the two counterpropagating laser beams. Saturated absorption by a ***standing wave*** laser field is observed when the axis of cat's eye coincides with the incident beam. The absorption by one travelling wave can be observed if the retroreflected beam is blocked before it reenters the atomic beam apparatus. The absorption is detected about one decay length downstream via the fluorescence emitted when the excited level decays into the ground state. The Ca oven has a temperature of approximately 930 K and an aperture of 0.5 mm diameter. An aperture of 1 mm diameter placed between the interacting zone and the PM determines the diameter of the Ca beam.

A typical saturation spectrum of the Ca intercombination line is shown in Fig. 25. In this example, the line was split by a magnetic field into three Zeeman components with $\Delta m_J = 0, \pm 1$. Consequently, we observe six components –three Zeeman components and the corresponding three crossover transitions. The central crossover line coincides with the central Zeeman component $\Delta m_J = 0$.

Fig. 26 shows measured saturation features observed at different laser powers for an excitation with a standing–wave field (a) and two counterpropagating travelling waves (b). The laser frequency was scanned from ν_0–1.5 MHz up to ν_0+1.5 MHz (ν_0: center frequency). In both cases the saturation dips have their largest depths at a laser power of about 2 mW. The saturation dip generated by two travelling waves is much deeper than that by a standing–wave and the relative depth size is even more than 50 %. The saturation dip generated by a standing–wave field becomes very small when the power increases to about 4 mW and turns into a peak at 6 mW. When the power is further increased, the total width of the (Doppler-)profile increases and two more peaks at both sides of the central peak appear P = 10 mW. At P = 20 mW, these peaks become even larger than the central peak. On the other hand, no peak was observed when the Ca beam was excited by two counterpropagating travelling waves.

Figure 27 shows the photocurrent measured at line center in dependence of the laser power for excitation with a standing wave (I_s), two counterpropagating travelling waves (I_2), and as a reference twice the signal of one travelling wave ($2I_1$). For laser powers between 1.2 mW and 4.5 mW, the photo–current I_2 generated by two travelling waves is smaller than that generated by one travelling wave. Consequently, the atomic beam

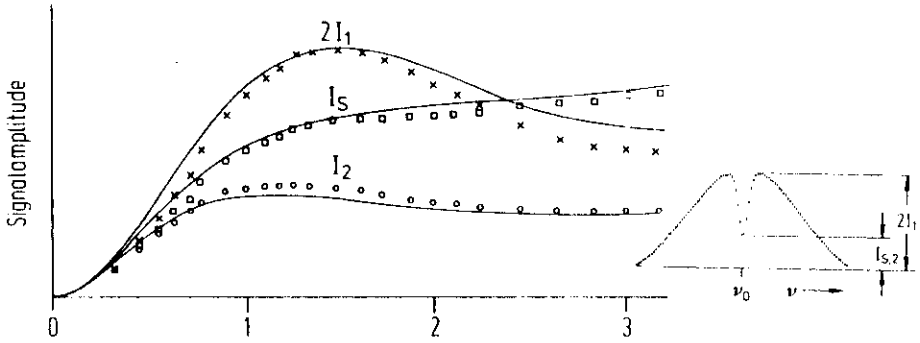

Fig. 27 Photocurrent measured and calculated vs laser power for a single travelling wave (I_1), two counterpropagating waves I_2 and a standing wave I_s.

absorbs more power from one travelling waves than from two counterpropagating waves field. On the other hand, if the laser power is larger than 4.5 mW, the photo–current for standing–wave excitation (I_s) is larger than for the reference ($2I_2$). In this case, the absorption of the standing wave is more than twice as large as that of one travelling wave and a peak appears instead of a saturation dip.

The experimental results described here are different compared to usual saturation spectroscopy. The difference is due to the lifetime of the exited state which is long compared to the transit-time and the inverse collision rate. In normal saturated absorption the lifetime of the excited state is shorter (due to collisions) and the ratio between the ground state and the excited state is usually determined by collisions. In such a case, the saturation can be described by a saturation parameter. In our experiment here, we need to consider only the interaction time and the transition probability. The origin of this strange line profile is not yet completely understood. We have verified the fluorescence signal observed at line center by solving the probability amplitude equations [1,3]. Basically, the features shown in Figs. 26 and 27 can be interpreted as demonstrations of Rabi-oscillations within the atomic beam. It is clear that different behavior is expected for standing waves due to the inhomogeneous field strength in the z direction and the corresponding inhomogeneous broadening of the Rabi-frequency in standing waves.

V. Optical Ramsey fringe spectroscopy

Utilizing conventional saturation spectroscopy, the observed linewidth is ultimately determined by the short interaction time of the thermal absorbers with laser light field. For atoms of the velocity v and for a radius w of the laser beam, such *transit-time broadening* is of the order of v/2w (in the range of 1 MHz for typical experimental conditions). It can be reduced by increasing the value of w [25]. With increasing beam diameters and the corresponding higher resolution however, the number of resonant atoms (given by v_z) decreases rapidly with increasing resolution and consequently the size of the Doppler-free signal is also reduced.

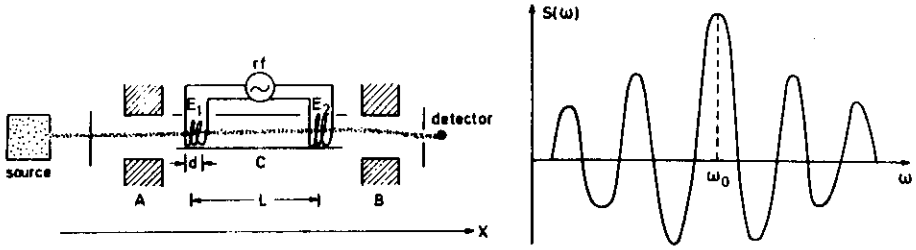

Fig. 28 Scheme of Ramsey excitation in the microwave range (a) and absorbed signal power vs frequency (b) (taken from [1]).

In general, the transit-time broadening can be largely reduced by applying the method of separated field excitation. It was first introduced to microwave spectroscopy by Ramsey [26] utilizing *two* interaction zones in an atomic beam (see Fig. 28). The atoms of an atomic beam pass sequentially through two excitation zones driven by the same oscillator of the frequency ω. In the first zone, a dipole moment between the ground state and the excited state is generated. In the field-free region this dipole precesses with the transition frequency ω_0. When it enters the second interaction zone, it has accumulated a phase angle $\Delta\varphi = \omega_0 T$ where $T = L/v$ is the flight-time of the atoms between the two interaction zones. In the same time, the phase of the field in the second has changed by $\omega T + \Delta\Phi$ where $\Delta\Phi$ represents a potential phase difference between the field in the two zones. The interaction between the dipole and the second zone depends on the phase difference $(\omega - \omega_0)T + \Delta\Phi$ between the precession and the exciting field.

For a mono-velocity atomic beam, we observe the signal

$$S(\omega) = CNE^2\cos[(\omega_0 - \omega)L/v + \Delta\Phi].$$

When the frequency of the oscillator is tuned $S(\omega)$ oscillates with a period of $\delta\nu = v/L$ (E: electric field, N: number of atoms passing through the interaction regions). The fringes wash out at higher detuning due to the transit-time broadening in *one* zone. In thermal beams with their wider velocity distribution the "side fringes" wash out even faster and only the central fringe and its next neighbors remain. The fringe width

$\delta\nu = \overline{v}/2L$ (FWHM) is determined by the time of flight between the two zones. It can be reduced by increasing the separation between the two zones. If we assume zero phase errors ($\Delta\Phi = 0$) and neglect the second order Doppler effect the observed Ramsey resonance structure is symmetrically distributed to the line center and can be used to determine the line center precisely. It should be noted that all primary atomic clocks apply the method of Ramsey's separated field excitation.

At *optical* frequencies with the lateral dimensions of the atomic beam being large compared to the wavelength, such two zone excitation would result in zero signals for single photon transitions. *Optical* Ramsey fringes, however, can be generated either by means of spatially modulated atomic beams [27] or by nonlinear excitation methods using more than two interaction zones [28].

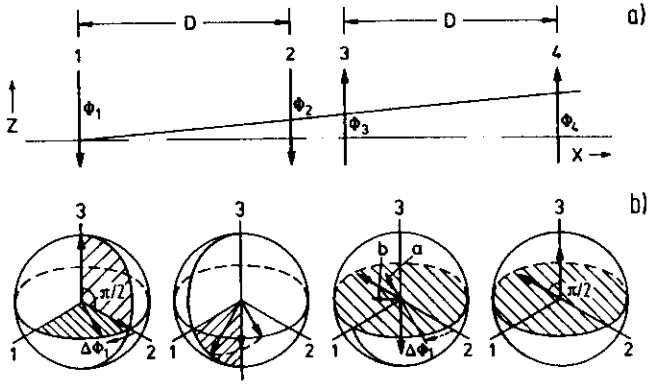

Fig. 29 a) Simplified scheme of optical Ramsey excitation by travelling waves; explanation of fringe generation using Bloch's formalism in the rotating wave approximation [29] ($\Phi_{1,2,3,4}$: phase of the light at z = 0).

Separated field excitation of optical transitions has been realized in one photon spectroscopy [28 – 34] utilizing standing and/or travelling waves. Fig. 29a shows schematically the Ramsey excitation with travelling waves of one atom out of a beam. The atom is excited sequentially by two pairs of parallel but counterpropagating laser beams. Following the theory of Bordé et al. [29], the generation of Ramsey fringes can be explained according to Fig. 29b by applying Bloch's formalism in the rotating wave approximation. In this figure, each of the four pictures correspond to one interaction. For the sake of simplicity, we assume the optimum condition that the pseudo spin [35] is rotated at each interaction by $\pi/2$ around the (1)–axis ($\pi/2$–pulse). During the first excitation, the pseudo spin is flipped from the (3)–direction –representing the population– into the (1,2)–plane representing the coherence between the initial and the excited states. In the field–free region between the first two laser beams, the spin rotates around the (3)–axis. The rotation angle at correct phase alignment $\Delta\Phi_1 = (\omega_0 v_z/c + \Delta\omega)D/v_x$ can be large compared to π depending on the Doppler shift $\omega_0 v_z/c$ and the detuning $\Delta\omega$ (v_z: component of atomic velocity in the z–direction of the laser beam). During the second excitation, the spin is rotated again around the (1)–axis into the (1,3)–plane. Correspondingly, the spin component in the (3)–direction will oscillate versus the velocity v_z and the detuning $\Delta\omega$. Summing over all v_z after the second excitation at an arbitrary fixed frequency would therefore give a zero fringe signal with the population of the atomic beam modulated in the v_z–space. (In the microwave range, such modulation does not exist due to the much larger wavelength and Ramsey fringes can be observed with two zones, only). The population modulation is then transferred to the next excitation zone where the atoms are interrogated with a laser beam (3) propagating in opposite direction. Due to the reversed beam direction, the phase of the pseudo spin is not conserved. The (3)–component of the pseudo–spin is again rotated into the (1,2)–plane by the laser field. For better understanding, the spin vector can now be split into the orthogonal components "a" and "b" with "a" pointing into the direction parallel or antiparallel to the spin direction $\Delta\Phi_1$ at the end of the first field–free region. Since the Doppler shift is reversed for the counter–propagating beams "3" and "4", the rotation of the phase is also reversed and the spin component "a" will coincide with the (2)–direction at the end of the third field–free region, independently of v_z. A macroscopic dipole moment will therefore exist at the location of the fourth excitation. The component "b", however, will average to zero after velocity integration. During the last excitation, the spin component "a" is eventually rotated into the (3)–direction

resulting in a nonlinear optical Ramsey interference. With the detuning of $\Delta\omega$, the phase of the coherence rotates by $\Delta\omega D/v_x$ around the (3)–direction both in the first and the third field–free space. Consequently, a periodic change of the population versus the frequency will appear. The total Ramsey structure will be obtained by summing over all atoms.

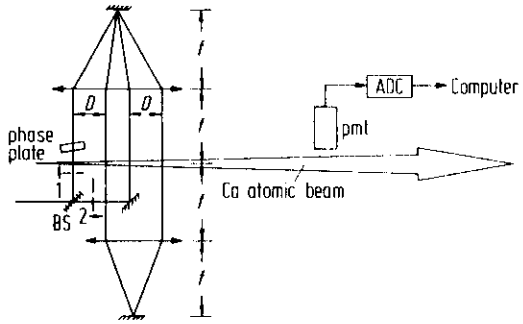

Fig. 30 Experimental setup for the detection of optical Ramsey fringes with travelling waves. Laser beam reversal is performed by stopping direction 1 or 2. The phase error $\Delta\Phi$ can be aligned by rotating the phase plate.

A typical setup for the detection of optical Ramsey fringes in a Ca atomic beam is shown in Fig. 30: An interaction geometry of four travelling waves is achieved by two cat's eyes providing phase alignment and precise retroreflection. The Ramsey signal can be detected by monitoring the fluorescence of the excited level versus the frequency. The corresponding signal $I_r(\omega)$ can then be written as

$$I_r(\omega) = \int_0^\infty A(P,t,\omega)\cdot f(v_x)\cdot \cos(2\Delta\omega D/v_x + \Delta\Phi)\cdot dv_x$$

where

$$\Delta\omega = \omega - \omega_0\left[1 - v^2/(2c^2) \pm \hbar\omega/(2mc^2)\right]$$

represents the detuning from the atomic resonance, $f(v_x)$ the velocity distribution and $A(P,t,\omega)$ the signal amplitude (depending on laser power P, interaction time t in one zone and weakly on the frequency ω). The terms $v^2/(2c^2)$ and $\hbar\omega/(2mc^2)$ describe frequency shifts caused by the second order Doppler effect and by the photon recoil. Since only the *first* but not the *second* order of the Doppler effect is suppressed by Doppler free methods, integration over all velocities leads to an inhomogeneous second order Doppler broadening and a shift of the Ramsey structure [36]. The photon recoil

causes a symmetric line splitting of $\hbar\omega^2/(mc^2)$ (typically a few kilohertz). The expression $\Delta\Phi = \Phi_2 - \Phi_1 + \Phi_4 - \Phi_3$ describes the phase error between the excitations. Neglecting the second order Doppler effect and the recoil splitting and assuming perfect phase alignment, the Ramsey signal can be described as a bilateral damped cosine. The center of the central fringe coincides with the atomic transition frequency and the fringe width of $\Delta\nu = v_x/(4D)$ (FWHM) is only determined by the excitation geometry. Principally, subnatural linewidth resolution is possible, however for the cost of reduced signal size.

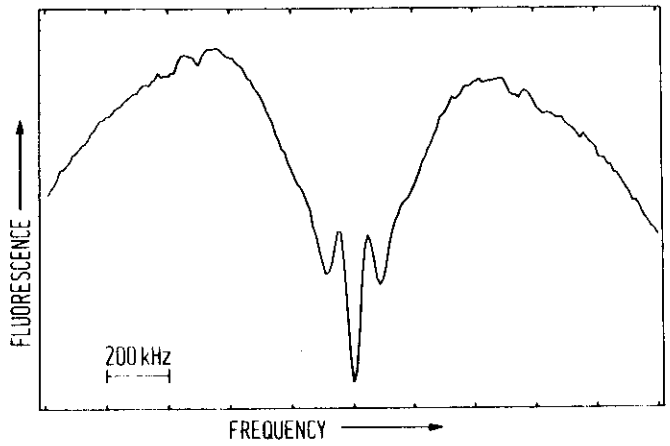

Fig. 31 Typical Ramsey signal observed in a Ca atomic beam.

A typical optical Ramsey structure observed by exciting a Ca atomic beam is shown in Fig. 31. The curve describes a Doppler–broadened atomic resonance with a Doppler–free Lamb–dip in the center. The Ramsey structure in turn appears in the center of the Lamb–dip. The Ramsey structure consists of a central fringe and a pair of side fringes. Higher order fringes are washed out due to the thermal velocity distribution of the Ca atoms.

Very narrow resonance structures can be achieved at large field separations and slow atomic velocities. The number of atoms contributing to the Ramsey structure is determined by the relatively small diameter of the laser beam in one excitation zone. Consequently, the signal size is largely increased at high resolution compared to conventional saturated absorption. At very high spectral resolution, comparable to the second order Doppler broadening however, Ramsey structures will be distorted and

shifted [36]. Consequently, the useful resolution and the uncertainty to determine the line center of thermal absorbers at rest is limited by second order Doppler broadening.

Velocity selection by pulsed excitation

The uncertainty caused by the second order Doppler effect can be reduced by selecting a narrow velocity interval of atomic absorbers if the light fields are pulsed (see Fig. 30). In these experiments [37], equal separations D between all four interactions were chosen. The light was chopped by means of an acoustooptic modulator.

The time of flight between the interactions can be determined conveniently by pulsing the laser radiation thereby selecting the velocity

$$v = D/(nT) \qquad n = 1,2,3,...$$

of the absorbers contributing to the Ramsey signal. The selected velocity interval is determined by the pulse width t and the radius w of the laser beam

$$\Delta v/v \leq [2/(3n)](2w/D+t/T)$$

The second order Doppler shift

$$\Delta\nu/\nu = (1/2)[D/(nTc)]^2$$

and broadening

$$\nu_b/\nu = [2/(3n)](D/nTc)^2(2w/D+t/T)$$

can then be calculated allowing the correction of the corresponding offsets. Fig. 32 shows

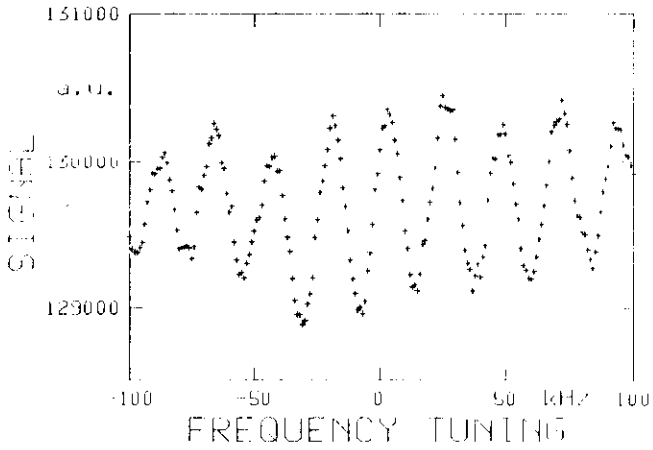

Fig. 32 Optical Ramsey fringes observed by pulsed separated field excitation in a Ca atomic beam. (D = 1.6 cm, T = 23 μs)

an example of Ramsey fringes observed with this method. Compared to the fringe signal of Fig. 31 observed at cw operation, the number of fringes is significantly increased due to the narrow velocity interval. The velocity distribution can be investigated by Fourier analyzing the fringe structure. Utilizing pulsed separated field excitation and suitable pulse separations T, only one single velocity interval (n = 1) contributed to the Ramsey signal. In this experiment, the second order Doppler broadening was decreased by approximately one order of magnitude to $9 \cdot 10^{-13}$. The contribution to the frequency uncertainty, caused by the second order Doppler effect can therefore be estimated to be below the 10^{-13} level.

Atomic beam cooling

The most rigorous approach to reduce transit-time broadening and the Doppler effect in all orders, is to increase the interaction time of the light with the absorbers by decreasing the kinetic energy of the absorbing particles. Such "cooling" can be performed by laser radiation applied to stored ions or atomic beams. In this chapter, the basics about laser deceleration of a Ca atomic beam will be discussed in view of applications to optical frequency standards.

Deceleration of atomic beams was first demonstrated by Andreev et al. [38]. It is accomplished by resonant laser radiation counter–propagating an atomic beam. During the cooling process, photons are continuously absorbed by the atomic beam and reemitted spontaneously. At each absorption process, the momentum of the absorbed photon $\hbar \cdot \omega/c$ is transferred to the atom in the direction of the laser beam whereas the reemission is randomly distributed in all directions. Consequently, there is a mean velocity reduction of $\hbar \cdot \omega/mc$ at each absorption process (m: atomic mass). For ^{40}Ca atoms excited from the $^1S_0$ ground state to the $^1P_1$ state (λ = 423 nm, lifetime of excited state: τ = 4.6 ns) the velocity change is 2.35 cm/s per event. The maximum deceleration rate a_{max} can be estimated under the assumption that the atoms spend half of their time in the excited state corresponding to a minimum cycling time of $2 \cdot \tau$

$$a_{max} = \hbar \cdot \omega/(2mc\tau).$$

The minimum time and length of deceleration are

$$T = \bar{v}/a_{max}$$

$$L = \bar{v}T/2,$$

respectively, with $\bar{v}$ being the mean velocity of the atomic beam. To stop ^{40}Ca atoms of 700 m/s velocity, we estimate $a_{max} = 2.55 \cdot 10^6$ cm/s², T = 0.3ms, L = 0.1m, and a saturation intensity of approximately 2 mW/mm². About 30000 absorption/emission cycles are necessary. Transversal heating of the beam can be reduced by a slightly converging laser beam.

During the deceleration, however, the Doppler shifted frequency of the atoms changes. The resonance condition is then no longer maintained and the cooling is interrupted. Consequently, only one velocity group of the total distribution will be transferred to its next smaller value (see Fig. 33). In order to cool and compress all velocity groups it is

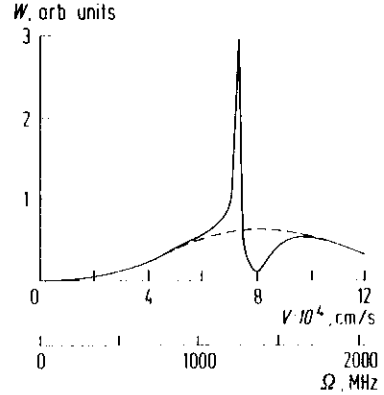

Fig. 33 Atomic velocity profile of a Na atomic beam produced by laser cooling at a constant frequency and constant magnetic field [38].

necessary to keep the transition frequency always in resonance with the decelerating absorbers. Such resonance condition can be maintained either by chirping the laser frequency or by Zeeman tuning the transition in a spatially varying dc magnetic field. Both methods have been realized using Na atomic beams [39,40]. Atomic beam cooling has also been demonstrated in other gases.

Deceleration of a Ca atomic beam has first been accomplished by F. Strumia et al. [41]. Fig. 34 shows a velocity profile of a Ca atomic beam cooled by a fixed laser frequency in a spatially varying magnetic field at PTB [42]. Curve a represents the unmodified velocity profile. Deceleration and velocity compression is clearly demonstrated.

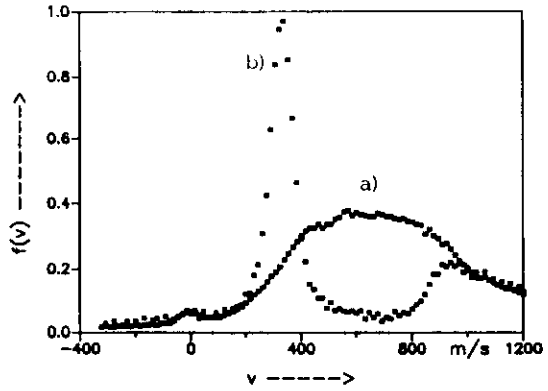

Fig. 34 Velocity profile of a laser cooled Ca atomic beam [42]

Atomic beam cooling presents a novel tool of precision laser spectroscopy. It opens the possibility, to confine atoms in shallow traps [43], to produce "optical molasses" [44], and "fountain geometries" [45]. Atomic beam deceleration is now ready to be applied to frequency metrology. It represents a powerful method for the development of optical frequency standards.

Influence of phase errors

Fig. 35 shows Ramsey fringe signals in dependence of the frequency for different separations D [33]: The width of the fringes decreases inversely with D. At D = 1cm, the splitting induced by the photon recoil effect [36] is partially resolved.

In these early experiments, the fringes at the highest resolution were distorted probably due to nonperfect alignment of the cat's eyes and residual phase errors. These problems have been addressed in the meantime leading to alignment procedures for the cat's eyes as well as for the phase correction [47]: The fine adjustment of the cat's eyes is tested –after interferometric prealignment– at the atomic beam, by monitoring the frequency shift of the Lamb–dip versus a parallel displacement of the laser beam from the optical axis. For perfect alignment, the center frequency should not depend on the displacement. Using this method, even small lense aberrations of the cat's eye can be observed and compensated. Residual small frequency shifts of the saturated absorption signal can be

compensated by laser beam reversal.

The dependence of the center frequency of Ramsey fringes upon the phase difference between the excitations has been investigated experimentally for traveling wave excitation [47]. Fig. 36 shows Ramsey fringe signals observed at various phase

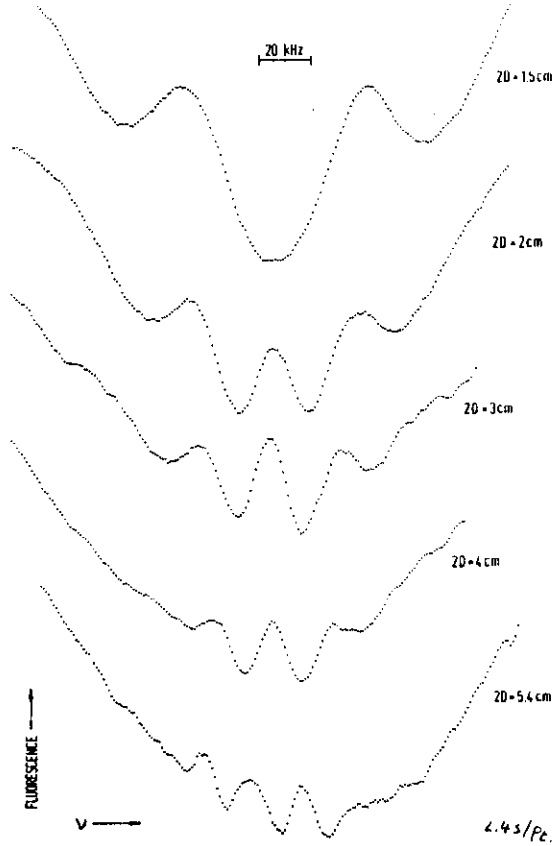

Fig. 35 Optical Ramsey resonances vs frequency observed in a Ca atomic beam for different separations D [33].

differences. The location of the Ramsey structure depends linearly on the phase difference $\Delta\Phi = \Phi_0 + n\delta\Phi$ ($n = 0, \pm 1, \pm 2, \ldots$). In the example shown in Fig. 36, the

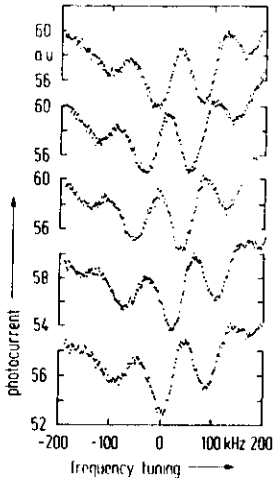

Fig. 36 Ramsey fringes observed with travelling waves (direction 1, see Fig. 30) for different settings of the phase plate (D = 0.75 cm, 0.5 s per point) [47].

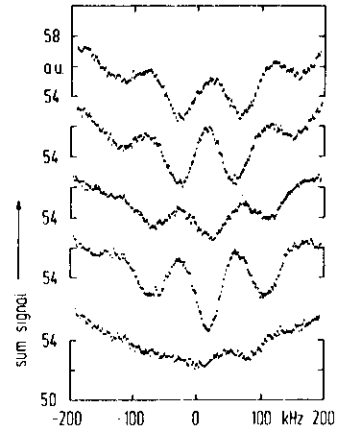

Fig. 37 Sum of optical Ramsey fringes observed in direction 1 and 2 (see Fig. 30) for different settings of the phase plate corresponding to Fig. 36.

fringes shift towards lower frequencies with increasing $\Delta\Phi$. If the laser beams are reversed, this shift also reverses and we expect symmetric, unshifted Ramsey fringes at each phase setting if the signals of the two directions are added. Such summed signals are shown in Fig. 37. The phase settings were the same as in Fig. 36. Within the experimental resolution (determined by the frequency stability of the laser and the signal to noise ratio), the center frequencies of the fringes do not change with $\Delta\Phi$, however, the fringe contrast changes through zero and fringe inversion occurs. Subtracting the two

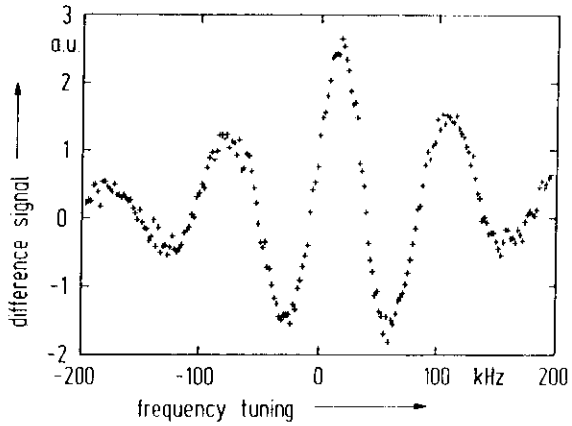

Fig. 38 Difference signal of the curves b and d in Fig. 37. Note that the background is suppressed.

inverted Ramsey signals of maximum contrast results in high contrast symmetrical Ramsey fringes free of background which are shown in Fig. 38.

Influence of the photon recoil

Fig. 39 shows a high resolution high contrast Ramsey structure. The fractional fringe width of approximately 2.10^{-11} (FWHM) is about 500 times narrower compared to that of the present primary standard of time and frequency. The peak to peak signal size is about 8% of the total fluorescence signal in this example. Fringe sizes up to 17% have been observed promising a fractional frequency instability of approximately $\sigma(2,\tau) \cong 6 \cdot 10^{-13} \cdot \tau^{-1/2}$ (with τ in s).

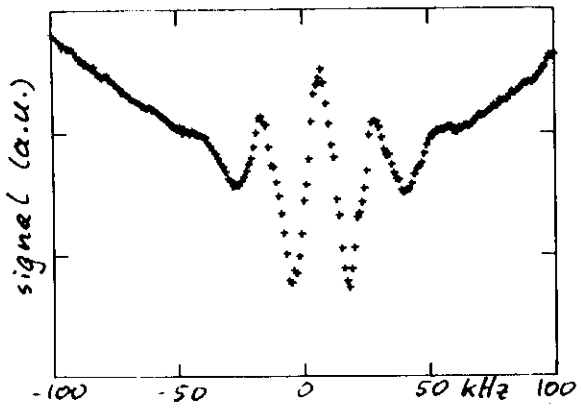

Fig. 39 Registration of a high contrast, high resolution Ramsey fringe signal (D = 2 cm) [47].

A serious problem to determine the true line center is caused by the recoil splitting in saturated absorption spectroscopy and in particular in Ramsey spectroscopy: At low resolution, the unresolved doublet structure may lead to line asymmetries caused by slightly different sizes and broadenings of the two components. At high resolution with the recoil components resolved, the signals will be strongly reduced in saturation spectroscopy or, with Ramsey excitation, the fringe signals will be distorted due to the 2nd order Doppler broadening of the thermal absorbers. On the other hand, utilizing cold absorbers of narrow velocity distribution and Ramsey excitation, the fringe signals of the two components will overlap due to the increased number of fringes [37]. One of the recoil components can be suppressed, by removing the population holes in the initial state (high frequency component) or the enhanced population in the upper state (low frequency component) in the atomic beam between the separated saturating and probing laser beams. Population decay of the upper state into a variety of other states was applied, for example, to iodine transitions [48,49]. However, the natural linewidth of the iodine transitions did not allow the suppression to be seen.

A novel method to suppress the low frequency recoil component uses optical pumping of the upper level into metastable states [50]. This method is very suitable for transitions to longlived excited states. In these experiments, suppression of the recoil component was demonstrated at the Ca intercombination line utilizing traveling wave Ramsey

excitation (see Fig. 30). The population of the $^3P_1$ state was pumped via the $^3S_1$–state into the metastable states $^3P_0$ and $^3P_2$ between the second and third interaction zone. The transit–time broadening was reduced to approximately 15 kHz. Fig. 40 shows the corresponding fringe signals a) without and b) with suppression of the low frequency recoil component. The Ramsey fringe signal of the low frequency component is essentially eliminated. Suppression of the low frequency recoil component was also

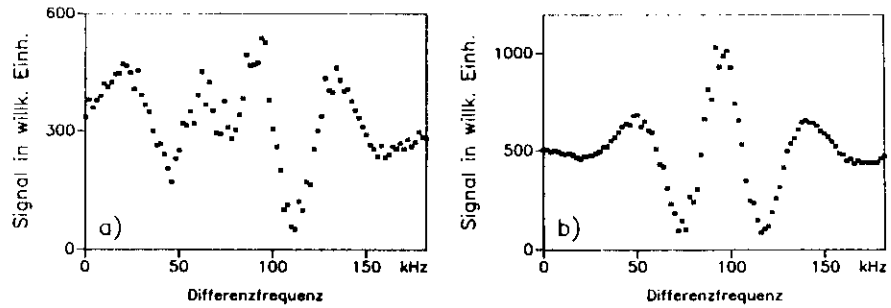

Fig. 40 High resolution Ramsey fringes observed in a Ca atomic beam a) without and b) with suppression of the low frequency recoil component

observed indirectly in saturated absorption using spatially separated large diameter laser beams: the width of the Lamb dip was reduced from about 60 kHz to approximately 40 kHz and its center was shifted by about 10 kHz towards higher frequencies. The described technique to excite only a single recoil avoids detrimental effects of the recoil splitting and can be used in any quantum system.

VI. Ca optical frequency standard

This chapter describes the PTB activities in the field of precision wavelength/frequency standards emitting visible radiation. The intercombination line $^3P_1$–$^1S_0$ of ^{40}Ca (λ = 657 nm) provides an attractive reference frequency for applications in optical frequency metrology [32]:

- the natural linewidth is in the range of only 400 Hz ($8 \cdot 10^{-13}$).
- ^{40}Ca has no hyperfine structure since its nuclear spin is zero.

–the ground state is not degenerated. Consequently, every atom can contribute to the signal.

–for transitions with $\Delta m_J = 0$, the transition frequency shows only a very small quadratic dependence on electric and magnetic fields of $1 Hz/(V/cm)^2$ and $10^8 Hz/T^2$, respectively.

–efficient, stable laser dyes are available at the atomic transition.

–atomic beam cooling is possible (see chapter V).

–a precise measurement of the transition frequency is in preparation.

–with the development of laser diodes operating in the visible range and their refinement to emit narrow linewidth and stable frequency, simple, low cost, Ca-stabilized lasers can be envisaged for practical length measurements and optical frequency transfer.

The necessary high resolution is achieved in our experiment by exciting optical Ramsey resonances in an atomic beam. Most of the investigations were carried out by traveling wave excitation as explained in chapter V but geometries with three standing waves [28] have also been used. The Ca atoms pass sequentially two pairs of traveling waves parallel but counter–propagating. The parallelism and the phase conditions are maintained by two cat's eyes, carefully focused. The cat's eyes also serve to project the beam waists at the axis of the atomic beam. Three zone standing wave excitation can be achieved by moving one of the retroreflectors parallel to the atomic beam.

In the first experiments, the dependence of the fringe position of the optical Ramsey resonance on $\Delta\Phi$ (see Fig. 36) has been used to develop a simple stabilization scheme using optical Ramsey fringes: The difference of two fringe signals corresponding to the two beam directions gives antisymmetric fringe signals free of background which are suitable as error signals for frequency stabilization. The maximum slope in the center is obtained if $\Delta\Phi = \pi/2$. Fig. 41a shows the signals for both beam directions "1" and "2" ($\Delta\Phi = \pi/2$). The difference of the two signals is depicted in Fig.41b. A dispersion–like signal free of background is clearly observed. We have stabilized our laser spectrometer utilizing the central zero crossing of curve b [46]: The observed error signal was used to servo-control the frequency of the synthesizer which in turn controls the dye laser frequency (see chapter II.).

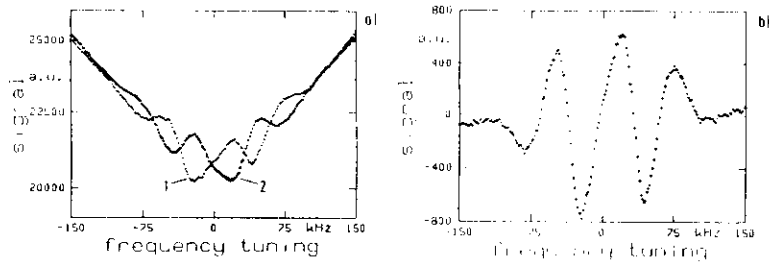

Fig. 41 Generation of an error signal for frequency stabilization by means of an optical Ramsey resonance. a) Curves 1 and 2: Ramsey structures observed at a fixed setting of the phase plate ($\Delta\Phi = \pi/2$) for laser beam directions 1 and 2 (see Fig. 30). b) Error signal generated by the difference of the two curves in a) [46].

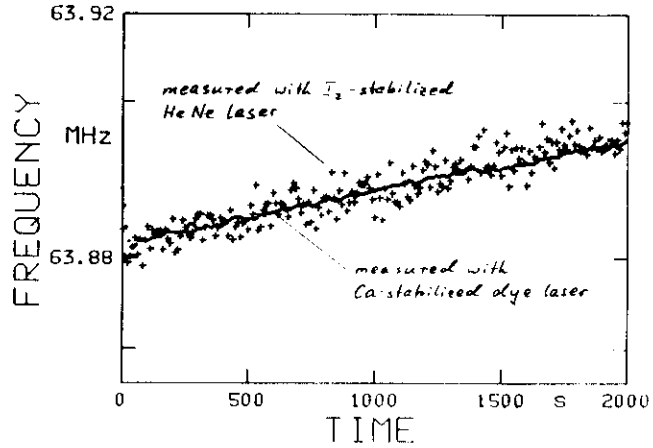

Fig. 42 Registration of the frequency drift of the reference resonator used in the dye laser spectrometer (see Fig. 12) measured a) with a "Ramsey-fringe stabilized" dye laser spectrometer and b) with a He-Ne laser [46].

As a first application of the "Ramsey-fringe stabilized" dye laser was used to monitor the small frequency drift of the optical reference resonator used in the dye laser spectrometer. Fig. 42 shows this drift measured with the "Ramsey fringe stabilized" dye laser (curve a) and with a He Ne offset laser (curve b, see also Fig. 11). A frequency drift of about 25 Hz/s was observed which is probably caused by slight heating of the resonator during the experiment. Both measurements show the same behavior of the resonator. However, the standard deviation of the measurements obtained with the dye–laser is much smaller, indicating that the useful resolution of our dye laser spectrometer is predominantly determined by the residual frequency instability of the I_2–stabilized He-Ne laser. At the present state the uncertainty of our Ca–stabilized dye laser to find the line center is estimated to be smaller than a tenth of a Ramsey fringe width, corresponding to a fractional uncertainty of about $2 \cdot 10^{-12}$ at maximum resolution. A second atomic beam has recently been constructed and used as a precision reference frequency for the spectrometer allowing improved studies of the reproducibility. Utilizing conventional saturated absorption for the stabilization, the frequency of the dye laser changes by less than 300 Hz, if the stabilization is switched from one atomic beam to the other one [51].

There has been significant improvement in the stabilization of lasers and development of precision optical frequency standards. The major limitations caused by the second order Doppler effect are being addressed in many laboratories investigating velocity selection and laser cooling. The most promising results are expected from optical frequency standards based on cooled and stored ions or slow atomic beams. At PTB, we are investigating laser cooling of a Ca beam. Slow Ca atoms will probably allow to decrease the uncertainties caused by phase errors and by the second order Doppler effect below the 10^{-14} level.

Presently, the uncertainty of optical frequency standards is mostly determined by the uncertainty to which optical frequencies can be measured. Most of the major steps to a frequency chain towards the visible have already been demonstrated in several laboratories. There is clearly an urgent need of phase–coherent optical frequency measurements. Precise knowledge of optical frequencies would provide significant impacts to frequency/wavelength metrology, precision optical spectroscopy, and determination of fundamental constants.

References

1. **W. Demtröder**: Laser Spectroscopy, Springer Series *Chemical Physics* 5 (Springer-Verlag, Berlin, Heidelberg, New York, 1982).
2. **K. Shimoda**: Line broadening and narrowing effects, in K. Shimoda (ed.) High–Resolution Laser Spectroscopy, Springer Series *Topics in Applied Physics* Vol. 13, (Springer-Verlag, Berlin, Heidelberg, New York 1976), p.11 – 49.
3. **V.S. Letokhov and V.P. Chebotayev**: *Nonlinear Laser Spectroscopy*, Springer Series in Optical Science, Vol.4, (Springer Berlin, Heidelberg, New York, 1977).
4. **F. Bayer-Helms, J. Helmcke**: *Modulation broadening of spectral profiles.* PTB-Bericht Me–17, (1977) 85-109 (in English).
5. **J.C. Bergquist, R.L. Barger, and D.J. Glaze**: *Laser Spectroscopy* IV, H. Walther, K.W. Rothe (eds.), Springer Ser. in Opt. Sci. 21, 120–129 (Springer Berlin, Heidelberg, New York, 1979).
6. **J. Helmcke, S.A. Lee, J.L. Hall**: Appl. Opt. 21, (1982) 1686 – 1694.
7. **J. Hough, D. Hils, M.D. Rayman, Ma L.–S., L. Hollberg, J.L. Hall**: Appl. Phys. B 33, (1984) 179.
8. **D. Hils, J.L. Hall**: in Proc. of the Symp. *Frequency standards and metrology*, A. de Marchi (ed.) (Springer-Verlag, Berlin, Heidelberg, New York, London, Paris, Tokyo 1989).
9. **R. Kallenbach, C. Zimmermann, D.H. McIntire, T.W. Hänsch, R.G. de Voe**: Opt. Comm. 70, (1989) 56.
10. **I. Steiner, V. Enders, F. Elsner, W. Neuhauser, P.E. Toschek, R. Blatt, J. Helmcke**: Appl. Phys. B 49, (1989) 251 – 256.
11. **J. Helmcke, J.J. Snyder, A. Morinaga, F. Mensing, M. Gläser**: Appl. Phys. B 43, (1987) 85 – 91.
12. **L.A. Hackel, D.G. Youmans, S. Ezekiel**: in J.H. Sanders, A.H. Wapstra (eds.) *Atomic masses and fundamental constants* 5, (Plenum Press, New York, London 1976), p.364 – 371.
13. **W.R. Bennett, Jr.**: Phys. Rev. 126, (1962) 580.
14. **G.R. Hanes, K.M. Baird, J. DeRemigis**: Appl. Opt. 12, (1973) 1600 – 1605
15. **A.J. Wallard**: J. Phys. B 5, (1972) 926 – 930.
16. **J.–M. Chartier, J. Helmcke, A.J. Wallard**: IEEE Trans. Instr. Meas IM–25, (1976) 450 – 453.

17. **R.B. Hurst, N. Brown, V.D. Dandawate, G.R. Hanes, J. Helmcke, H.P. Layer, Liu Zhongyou, W.R.C. Rowley, M.S. Chung**: Metrologia 24, (1987) 39 – 44.
18. **S. Iwasaki, J.–M. Chartier**: Metrologia 26, (1989) 257 – 261.
19. **G.C. Bjorklund**: Opt. Lett 5, (1980) 15 – 17.
20. **J.L. Hall, L. Hollberg, Ma Long–sheng, T. Baer, H.G. Robinson**: J. de Phys. C8, Suppl. 12, Tome 42, (1981) 59 – 71.
21. **J.J. Snyder, R.K. Raj, D. Bloch, M. Ducloy**: Opt. Lett. 163 – 165.
22. **U. Brand**: to be published.
23. **U. Brand, J. Helmcke**: Proc of the Symp. *Frequency standards and metrolgy*, A. De Marchi (ed.) (Springer-Verlag Berlin, Heidelberg 1989), 467 – 468.
24. **J. Ishikawa, F. Riehle, J. Helmcke**: to be published.
25. **Ch.J. Bordé, J.L. Hall, C.V. Kunasz, and D.G. Hummer**: Phys. Rev. A 14, (1976) 236 – 263.
26. **N.F. Ramsey**: Molecular Beams (Oxford University Press, London 1956) Chap. 2.
27. **G. Kramer**: J. Opt. Soc. Am. 68, 1634 (1978).
28. **Ye.V. Baklanov, B.Ya. Dubetsky, V.P. Chebotayev**: Appl. Phys. 9, 171 (1976).
29. **Ch.J. Bordé, Ch. Salomon, S. Avrillier, A. van Lerberghe, Ch. Bréant**: Phys. Rev. A 30, (1984) 1836.
30. **M. Baba, K. Shimoda**: Appl. Phys. 24, (1981) 11.
31. **J.C. Bergquist, S.A. Lee, J.L. Hall**: in Laser Spectroscopy III, Springer Ser. Opt. Sci. 7 (Springer, Berlin, Heidelberg, N.Y.) J.L. Hall, J.L. Carlsten, eds., p. 142 (1977).
32. **J.C. Bergquist, R.L. Barger, D.J. Glaze**: in Laser Spectroscopy IV, Springer Ser. Opt. Sci. 21, (Springer, Berlin, Heidelberg, N.Y.), H. Walther, K.W. Rothe, eds., p. 120 (1979).
33. **J. Helmcke, D. Zevgolis, B.Ü. Yen**: Appl. Phys. Lett. B–28, (1982) 83.
34. **G. Camy, N. Courtier, J. Helmcke**: in Laser Spectroscopy VIII, Springer Ser. Opt. Sci. 55, (Springer, Berlin, Heidelberg, N.Y.) W. Persson, S. Svanberg, eds., p. 386 (1987).
35. **R.P. Feynman, F.L. Vernon**: J. Appl. Phys. 28, (1957) 49.
36. **R.L. Barger**: Opt. Lett. 6, (1981) 145.
37. **H. Hellwig, S. Jarvis, D.J. Glaze, D. Halford, H.E. Bell**: Proc. 27th Annual Symp. on Frequ. Contr., Fort Monmouth, N.J., p. 357 (1973) and
A. Morinaga, J. Helmcke: Appl. Phys. B 45 (1988) 273 – 277.
38. **S.V. Andreev, V.I. Balykin, V.S. Letokhov, V.G. Minogin**: Pis'ma Zh. Eksp. Teor. Fiz. 34, (1981) 463 – 467 [JETP Lett. 34, (1981), 442 – 445].

39. **W.D. Philips, H. Metcalf**: Phys. Rev. Lett. 48, (1982) 596.
40. **W. Ertmer, R. Blatt, J.L. Hall, M. Zhu**: Phys. Rev. 54, (1985) 996.
41. **N. Beverini, F. Giammanco, E. Maccioni, F. Strumia, G. Vissani**: Ninth Int. Conf. on Laser Spectroscopy, Bretton Woods, USA, (1989) Academic Press, in press.
42. **Th. Kisters, A. Witte, J. Ishikawa, Liu Li., F. Riehle, J. Helmcke**: to be published.
43. **A.L. Migdall, J.V. Prodan, W.D. Phillips, T.H. Bergeman, H.J. Metcalf**: Phys. Rev. Lett. 54, (1985) 2596.
44. see for example: **S. Chu, M.G. Prentiss, E.A. Cable, J.E. Bjorkholm**: Laser Spectroscopy VIII, Springer Ser. Opt. Sci. 55 (Springer, Berlin, Heidelberg, N.Y.), W. Persson, S. Svanberg, eds., p.58 (1987).
45. **M.A. Kasevich, E. Riis, S. Chu, R.G. DeVoe**: Phys. Rev. Lett. 63, (1989) 612 – 615.
46. **A. Morinaga, F. Riehle, J. Ishikawa, J. Helmcke**: Appl. Phys. B 48, (1989) 165 – 171.
47. **J. Helmcke, A. Morinaga, J. Ishikawa, F. Riehle**: IEEE Trans Instr Meas. 38, (1989) 524 – 532.
48. **A.N. Gonchorov, M.N. Skortsov, V.P. Chebotayev**: Sov. J. Quant. Electr. 13, (1983) 1492.
49. **G. Camy, N. Courtier, J. Helmcke**: in *Laser Spectroscopy*, W. Persson, S. Swanberg (eds.) (Springer–Verlag, Berlin, 1987), p. 386.
50. **F. Riehle, J. Ishikawa, J. Helmcke**: Phys. Rev. Lett. 61, (1988) 2092 – 2095.
51. **J. Ishikawa, F. Riehle, J. Helmcke**: to be published.